ISSN 1674-1056
http://cpb.iphy.ac.cn
http://iopscience.iop.org/cpb
中国物理 B
Chinese Physics
中国物理 Chinese Physics B

Ground-state vortex structures of a rotating binary dipolar Bose-Einstein condensate confined in harmonic plus quartic potential

Guang-Ping Chen(陈光平), Chang-Bing Qiao(乔昌兵), Hui Guo(郭慧), Lin-Xue Wang(王林雪), Ya-Jun Wang(王雅君), Ren-Bing Tan(谭仁兵)

Citation: Chin. Phys. B . 2019, 28(1): 010308. **doi:** 10.1088/1674-1056/28/1/010308
Journal homepage: http://cpb.iphy.ac.cn; http://iopscience.iop.org/cpb

What follows is a list of articles you may be interested in

Trapped Bose-Einstein condensates with quadrupole-quadrupole interactions

An-Bang Wang(王安邦), Su Yi(易俗)
Chin. Phys. B . 2018, 27(12): 120307. **doi:** 10.1088/1674-1056/27/12/120307

Tunable ground-state solitons in spin-orbit coupling Bose-Einstein condensates in the presence of optical lattices

Huafeng Zhang(张华峰), Fang Chen(陈方), Chunchao Yu(郁春潮), Lihui Sun(孙利辉), Dahai Xu(徐大海)
Chin. Phys. B . 2017, 26(8): 080304. **doi:** 10.1088/1674-1056/26/8/080304

The ground states and pseudospin textures of rotating two-component Bose-Einstein condensates trapped in harmonic plus quartic potential

Yan Liu(刘燕), Su-Ying Zhang(张素英)
Chin. Phys. B . 2016, 25(9): 090304. **doi:** 10.1088/1674-1056/25/9/090304

Generating periodic interference in Bose-Einstein condensates

Shen-Tong Ji(冀慎统), Yuan-Sheng Wang(王元生), Yue-E Luo(罗月娥), Xue-Shen Liu(刘学深)
Chin. Phys. B . 2016, 25(9): 090303. **doi:** 10.1088/1674-1056/25/9/090303

Weakly interacting spinor Bose-Einstein condensates with three-dimensional spin-orbit coupling

Shu-Wei Song(宋淑伟), Rui Sun(孙蕊), Hong Zhao(赵洪), Xuan Wang(王暄), Bao-Zhong Han(韩宝忠)
Chin. Phys. B . 2016, 25(4): 040305. **doi:** 10.1088/1674-1056/25/4/040305

Ground-state vortex structures of a rotating binary dipolar Bose–Einstein condensate confined in harmonic plus quartic potential*

Guang-Ping Chen(陈光平)[1,†], Chang-Bing Qiao(乔昌兵)[2], Hui Guo(郭慧)[3,4], Lin-Xue Wang(王林雪)[3,4], Ya-Jun Wang(王雅君)[3,4], and Ren-Bing Tan(谭仁兵)[5]

[1] *School of Intelligent Manufacturing, Sichuan Art and Science University, Dazhou* 635000, *China*
[2] *School of Chemistry and Chemical Engineering, Sichuan Art and Science University, Dazhou* 635000, *China*
[3] *Key Laboratory of Time and Frequency Primary Standards, National Time Service Center, Chinese Academy of Sciences, Xi'an* 710600, *China*
[4] *School of Astronomy and Space Science, University of Chinese Academy of Sciences, Beijing* 100049, *China*
[5] *College of Mathematics and Physics, Chongqing University of Science and Technology, Chongqing* 401331, *China*

(Received 26 June 2018; revised manuscript received 8 November 2018; published online 21 December 2018)

We consider a binary dipolar Bose–Einstein condensate confined in a rotating harmonic plus quartic potential trap. The ground-state vortex structures are numerically obtained as a function of the contact interactions and the dipole–dipole interaction in both slow and rapid rotation cases. The results show that the vortex configurations depend strongly on the strength of the contact interactions, the relative strength between dipolar and contact interactions, as well as on the orientation of the dipoles. A variety of exotic ground-state vortex structures, such as pentagonal and hexagon vortex lattice, square vortex lattice with a central vortex, annular vortex lines, and straight vortex lines, are observed by turning such controllable parameters. Our results deepen the understanding of effects of dipole–dipole interaction on the topological defects.

Keywords: Bose–Einstein condensate, dipolar–dipolar interaction, harmonic plus quartic potential trap, vortex structure

PACS: 03.75.Lm, 03.75.Mn, 05.30.Jp **DOI:** 10.1088/1674-1056/28/1/010308

1. Introduction

During the past decades, topological defects, such as quantized vortices,[1,2] skyrmions,[3,4] and merons,[5,6] have attracted a lot of interest in many branches of physics ranging from condensed matter to high-energy physics. The successful realization of multi-component Bose–Einstein condensate (BEC) in experiment offers us an effective platform to study such defects due to the highly controllable parameters.[7] Various ground-state structures and dynamic properties are presented in the two-component BEC system.[8–11]

Recently, the dipolar BECs with large magnetic moment atomic species have been realized successfully in practical experiments.[12–15] Different from the isotropic contact interaction, the dipole–dipole interaction (DDI) is anisotropy, and not only attractive but also repulsive, relying on the angle θ between the polarization axis and the vector $\boldsymbol{r}$ between the two dipoles. The DDI has been discussed as an important tool for studying multibody physics, which provides means for quantum computation, quantum magnetism simulation, and the realization of various topological defects.[16,17]

In practical experiments, BECs are usually confined by external potential; the ground-state and dynamics properties of BEC are significantly affected by different shapes of external potential. Very recently, a binary dipolar condensate, which consists of dipolar and scalar atoms, has drawn considerable attention. However, most of the previous studies have focused on harmonic potential,[18,19] optical lattice,[20–23] toroidal trap,[24] concentrically coupled annular trap,[25,26] and so on. In such situations, a large number of exotic ground-state structures are observed due to the presence of DDI. The only drawback of such potential lies in the fact that the rotational frequency cannot exceed the frequency of radial trap oscillator, and thus one cannot reach the fast rotation region.

In this paper, we are interested in a typical toroidal trap, which is known as the Mexican hat potential and consists of a harmonic plus quartic potential.[27,28] The ground-state of a two-component miscible BEC confined in this trap has been studied in Ref. [29]. Soon after that, the ground-state properties of Rashba spin–orbit-coupled spin-1/2 BEC in the same trap have been studied by Wang *et al.*[30] In what follows, we will study the ground-state properties of a rotating dipolar BEC confined in this harmonic plus quartic potential trap, and investigate the effects of strength and orientation of DDI, contact interaction, and rotation on the vortex properties of dipolar BEC.

*Project supported by the Sichuan Province Education Department Key Natural Science Fund, China (Grant No. 17ZA339), the Chongqing Research Program of Basic Research and Frontier Technology, China (Grant No. cstc2014jcyjA50016), and the National Natural Science Foundation of China (Grant No. 61504016).
†Corresponding author. E-mail: chengp205@126.com
© 2019 Chinese Physical Society and IOP Publishing Ltd

The rest of this paper is organized as follows. The theoretical model describing a quasi-two-dimensional (Q2D) binary rotating BEC under the harmonic plus quartic trap is introduced in Section 2. The main numerical results of the ground-state vortex structures under both slow rotation and rapid rotation are presented in Section 3. Finally, the main conclusions are summarized in Section 4.

2. Theory model

We begin with a rotating binary dipolar BEC, which contains atoms with magnetic dipoles (denoted by component 1) and scalar atoms (denoted by component 2), and is confined to a Q2D harmonic plus quartic trap in the x–y plane. Within the framework of zero-temperature mean-field theory, the ground state and dynamics of such a system can be well described by the following coupled Gross–Pitaevskii (GP) equations

$$\begin{aligned}
&\mathrm{i}\hbar\partial\psi_1(r,t)/\partial t\\
&= \Big[-\frac{\hbar^2}{2m_1}\nabla^2+V(r)+U_{11}|\psi_1(r,t)|^2+U_{12}|\psi_2(r,t)|^2\\
&\quad -\Omega L_z+\int U_{\mathrm{dd}}(r-r')\left|\psi_1(r',t)\right|^2\mathrm{d}r'\Big]\psi_1(r,t),\\
&\mathrm{i}\hbar\partial\psi_2(r,t)/\partial t\\
&= \Big[-\frac{\hbar^2}{2m_2}\nabla^2+V(r)+U_{21}|\psi_1(r,t)|^2\\
&\quad +U_{22}|\psi_2(r,t)|^2-\Omega L_z\Big]\psi_2(r,t),
\end{aligned}\tag{1}$$

where m_i is the atomic mass of component i, and we simply assume that the masses of the two component atoms are equal as $m_1=m_2=m$; Ω is the effective rotation frequency of the system. The coefficients $U_{11}=U_{22}=4\pi\hbar^2a_{11}/m$ and $U_{21}=U_{12}=4\pi\hbar^2a_{12}/m$ are the intra- and inter-component interaction strengths, where a_{ii} is the corresponding s-wave scattering length between atoms. $L_z=-\mathrm{i}\hbar(x\partial_y-y\partial_x)$ is the orbital angular momentum of z-component. The wave functions are normalized as $\int(|\psi_1(r,t)|^2+|\psi_2(r,t)|^2)\mathrm{d}r=N$ with N being the total number of atoms in condensate.

When all dipoles are polarized along the same direction by an external field, the explicit dipole–dipole interaction reads[15]

$$U_{\mathrm{dd}}(r-r')=\frac{C_{\mathrm{dd}}}{4\pi}\frac{1-3\cos^2\theta}{|r-r'|^3},\tag{2}$$

where $C_{\mathrm{dd}}=\mu_0\mu^2$ describes the strength of the DDI for magnetic dipoles, with μ_0 and μ respectively being the vacuum magnetic permeability and the dipole moment of the atoms. θ is the angle between the polarization axis and the vector $\boldsymbol{r}$ between the two dipoles. The external potential which is known as the Mexican hat potential can be written as[27]

$$\begin{aligned}
V(r) &= \frac{1}{2}m\omega_\perp^2\left[V_0\left(\frac{r^2}{a_0}-a_0r_0\right)^2\right]\\
&= \frac{1}{2}\hbar\omega_\perp\left[V_0\left(\frac{r^2}{a_0^2}-r_0\right)^2\right],
\end{aligned}\tag{3}$$

where $\omega_\perp$ is the radial oscillation frequency, $a_0=\sqrt{\hbar/m\omega_\perp}$ is the oscillator length, V_0 and r_0 are dimensionless constants, and $r=\sqrt{x^2+y^2}$ is the radial coordinate. The lowest point of the trap is $(\pm a_0r_0,\ 0)$, and the highest center point of the trap is $(0,\ \hbar\omega_\perp V_0r_0^2/2)$. Without loss of generality, we are particularly concerned about the case with $V_0=0.5$ and $r_0=5$ by introducing the scales characterizing the trapping potential: the length a_0, and time $1/\omega_\perp$, which can also be realized in real experiments. Therefore, the dimensionless coupled GP equations can be rewritten as

$$\begin{aligned}
\mathrm{i}\frac{\partial\psi_1}{\partial t} &= \Big(-\frac{1}{2}\nabla^2+V+\beta_{11}|\psi_1|^2\\
&\quad +\beta_{12}|\psi_2|^2+\Phi_{\mathrm{dd}}-\Omega L_z'\Big)\psi_1,\\
\mathrm{i}\frac{\partial\psi_2}{\partial t} &= \Big(-\frac{1}{2}\nabla^2+V+\beta_{21}|\psi_1|^2\\
&\quad +\beta_{22}|\psi_2|^2-\Omega L_z'\Big)\psi_2,\\
\Phi_{\mathrm{dd}} &= \frac{N\mu_0\mu^2}{4\pi\hbar\omega_\perp a_0^3}\int\frac{1-3\cos^2\theta}{|r-r'|^3}\left|\psi_1(r')\right|^2\mathrm{d}r',
\end{aligned}\tag{4}$$

where $\beta_{ii}=4\pi a_iN$ and $\beta_{12}=\beta_{21}=2\pi a_{12}N$ are corresponding to the strengths of intra- and inter-component interactions, respectively. The dimensionless wave functions are normalized as $\int(|\psi_1(r,t)|^2+|\psi_2(r,t)|^2)\mathrm{d}r=1$. $L_z'=-\mathrm{i}(x\partial_y-y\partial_x)$ is the dimensionless orbital angular momentum of z-component and $\varepsilon_{\mathrm{dd}}=a_{\mathrm{dd}}/a_{\mathrm{s}}=\frac{\mu_0\mu^2m}{12\pi\hbar^2a_{\mathrm{s}}}$, where a_{s} is the s-wave scattering length for contact interaction of dipolar component; hence a_{dd} can be interpreted as "dipole length", which is defined as $a_{\mathrm{dd}}=C_{\mathrm{dd}}m/(3\hbar^2)$.[31] The DDI provides an attractive interaction in the case of $\varepsilon_{\mathrm{dd}}<0$, and vice versa. Meanwhile, for $\varepsilon_{\mathrm{dd}}<1$, the short-range part of intra-component interaction dominates and the DDI provides a correction; however, for large values of $\varepsilon_{\mathrm{dd}}>1$, the long-range DDI dominates, and the strong restriction of the quartic potential will prevent the system from collapsing; it can keep the system stable even though the DDI reaches to 3.

3. Results and discussion

By numerically solving the dimensionless coupled GP Eq. (4), we can obtain the ground-state vortex structures of the system within an imaginary-time propagation approach.[32,33] We prepare reasonable initial wave functions for such two components, and then propagate such functions in imaginary time to reach a stable state. We have to note that in the presence of quartic trap, although the rotation frequency is larger than the confined oscillator frequency of harmonic potential, the BEC can keep stable for the strong confinement of quartic trap; in other words, we can study the ground state of

this system for both slow rotation ($\Omega < 1$) and rapid rotation ($\Omega > 1$). Meanwhile, the DDI introduces another controllable parameter, which leads to a much larger parameter space. Therefore, we can expect that a variety of exotic vortex structures will be exhibited in this system. Without loss of generality, in this paper, we try to simplify the situation by choosing equivalent intra-component interaction constants as $\beta = \beta_{11} = \beta_{22} = 100$ and investigate various ground-state vortex structures as a function of inter-component interaction β_{12}, DDI, and the rotation frequency. In what follows we first study the slow rotation case, and then move to the rapid rotation case.

3.1. The ground-state vortex structures for slow rotation

We begin with the case of slow rotation. Figure 1 shows the density and phase distributions of the system for different inter-component interactions and DDIs. We can consider the condition of $\theta = \pi/2$ firstly; under this condition, the DDI is purely repulsive and isotropic. In the absence of DDI, the system shows phase coexistence or phase separation, depending on whether $\beta_{11}\beta_{22} < \beta_{12}^2$ or $\beta_{11}\beta_{22} > \beta_{12}^2$. Typical examples are shown in the first column of Fig. 1(a) for $\beta_{12} = 50$ and $\beta_{12} = 250$, corresponding to the first and third rows, respectively. For the coexistence case, both the dipolar and scalar components are mixed and circularly distributed around the lowest potential energy point ($r = \pm r_0$). In addition, three hidden vortices are formed at the center of the circles in the two components. When the DDI is introduced and takes a small value, such as $\varepsilon_{dd} = 1$, the effective repulsive interaction in dipolar component increases, and its density expands to the outside and inside. Compared with the scalar component, three hidden vortices in the dipolar component are separated from each other, as shown in the second row of Fig. 1(b). Increasing the DDI to $\varepsilon_{dd} = 2$ (see the first two rows of Fig. 1(c)), the density distribution of dipolar component is further expanded. In this case, five visible vortices appear in the dipolar component, and a central vortex is surrounded by four vortices. For a larger value of DDI, such as $\varepsilon_{dd} = 4$, the density and phase distribution are shown in the top two rows of Fig. 1(d), where the central vortex is destroyed by the strong repulsion of dipolar component, and the other four vortices are distributed as square vortex structure.

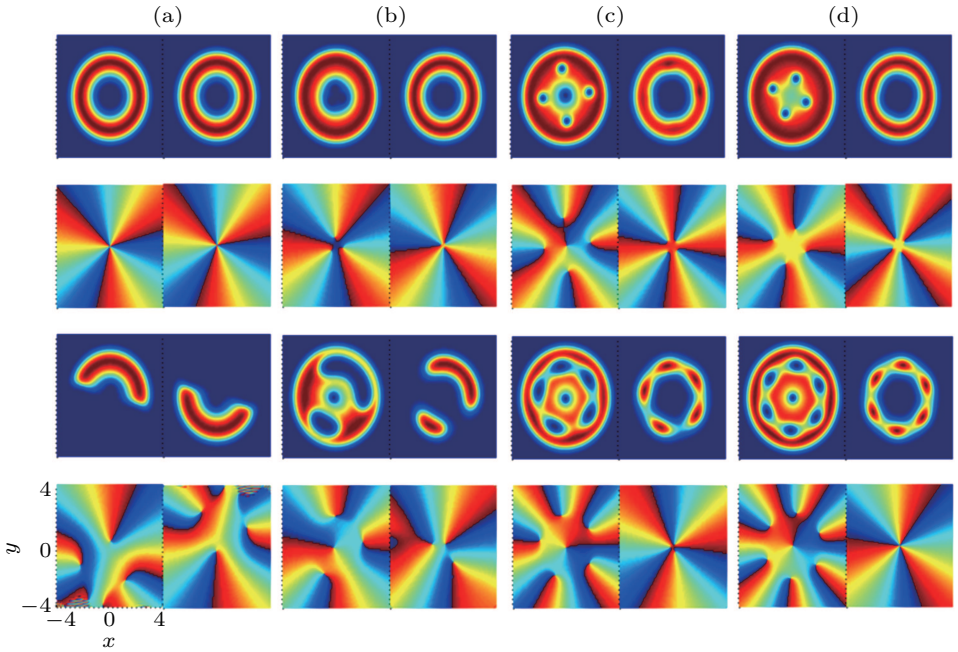


Fig. 1. Typical two-dimensional atomic density and phase profiles of slow rotation for different inter-component interactions ($\beta_{12} = 50$ in the top two rows and $\beta_{12} = 250$ in the bottom two rows) and DDIs. The strengths of dipolar interaction are set as (a) $\varepsilon_{dd} = 0$, (b) $\varepsilon_{dd} = 1$, (c) $\varepsilon_{dd} = 2$, and (d) $\varepsilon_{dd} = 4$ for the top two rows, and (a) $\varepsilon_{dd} = 0$, (b) $\varepsilon_{dd} = 2$, (c) $\varepsilon_{dd} = 3$, and (d) $\varepsilon_{dd} = 4$ for the bottom two rows. Other parameters are set as $\Omega = 0.7$ and $\theta = \pi/2$.

For the phase separation case ($\beta_{12} = 250$), the density and phase distribution are shown in the bottom two rows of Fig. 1. The dipolar component and scalar component atoms are separated from each other due to the strong repulsion between the two components without DDI, which is shown in Fig. 1(a). In the presence of DDI ($\varepsilon_{dd} = 2$), the density of scalar component is separated to two parts and surrounded by the dipolar component, and the density of dipolar component is expanded and forms a central visible vortex. If we increase the DDI to larger values as $\varepsilon_{dd} = 3$ and $\varepsilon_{dd} = 4$, which are shown in the bottom two rows of Figs. 1(c) and 1(d), respectively, the density of scalar component forms an annulus distribution and is surrounded by the dipolar component. Similar to the phase coexistence case, the effective repulsive interaction of dipolar component increases with the increase of the DDI. Moreover, the hidden vortices in the dipolar component become visible

and form regular vortex lattices with a central vortex, such as pentagon and hexagon.

3.2. The ground-state vortex structures for rapid rotation

We now move to the case of rapid rotation $\Omega = 2.5$. For the phase coexistence case and in the absence of DDI (see Fig. 2(a)), both dipolar and scalar component atoms are distributed in the lowest potential energy of annulus, which is similar to the first row of Fig. 1(a). But the scope of density area is much narrower than that in Fig. 1(a). Moreover, we can see that the number of hidden vortices is much larger than that in Fig. 1(a) too. When the DDI is introduced and increased to $\varepsilon_{\rm dd} = 1$, typical density and phase distributions are shown in the top two rows of Fig. 2(b). On the one hand, the annular condensate of dipolar component becomes wider, and on the other hand, most of the hidden vortices move from the center of the annular condensate to the inner edge. Meanwhile, some of them become visible and form a vortex ring in the annular condensate. We have to note that although some of the hidden vortices in the scalar component are also moving outward, the condensate is compressed too thin to form visible vortices. As the DDI increases to $\varepsilon_{\rm dd} = 2$, shown in the top two rows of Fig. 3(c), a visible vortex ring is formed in the annular condensate of dipolar component. Interestingly, a hidden vortex ring, together with a high-order hidden vortex, is formed in the central region. However, the scalar component atoms form a robust annular stripe condensate in the place of the visible vortex ring of the dipolar condensate. This robustness of the annular stripe condensate actually prevents the movement of its own vortices and the formation of visible vortices. Finally, if the DDI increases to an even larger value, such as $\varepsilon_{\rm dd} = 4$, shown in the top two rows of Fig. 2(d), the number of visible vortices in dipolar component further increases, and more and more visible vortices are formed in the annular condensate. However, the scalar component is also compressed into an annular stripe condensate with hidden vortices.

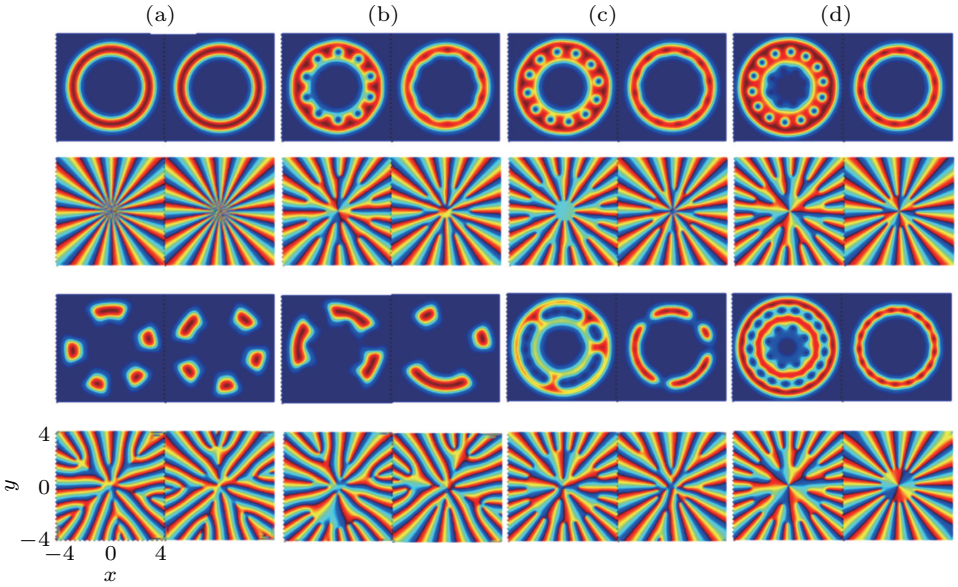


Fig. 2. The typical two-dimensional atomic density and phase profiles of the slow rotation case for different inter-component interactions ($\beta_{12} = 50$ for the top two rows and $\beta_{12} = 250$ for the bottom two rows) and DDIs. The strengths of dipolar interaction are set as (a) $\varepsilon_{\rm dd} = 0$, (b) $\varepsilon_{\rm dd} = 1$, (c) $\varepsilon_{\rm dd} = 2$, and (d) $\varepsilon_{\rm dd} = 4$ for the top two rows, and (a) $\varepsilon_{\rm dd} = 0$, (b) $\varepsilon_{\rm dd} = 0.3$, (c) $\varepsilon_{\rm dd} = 2$, and (d) $\varepsilon_{\rm dd} = 4$ for the bottom two rows. Other parameters are set as $\Omega = 2.5$ and $\theta = \pi/2$.

The bottom two rows of Fig. 2 show the vortex structures and its associated phase profiles for a larger value of inter-component interaction $\beta_{12} = 250$. In the absence of DDI (see Fig. 2(a)), the dipolar and scalar component are distributed in the lowest potential energy area, but both of them are separated into five lumps and alternately arranged. When a small DDI ($\varepsilon_{\rm dd} = 0.3$) is introduced (see Fig. 2(b)), the density distributions of the two components are melt into three lumps. Further increasing the DDI to $\varepsilon_{\rm dd} = 2$ (see Fig. 2(c)), a novel vortex structure is formed, the dipolar component forms a shell, and the empty parts of the annular dipolar component are filled by the scalar component. In the meantime, the vortices of dipolar component are located in the empty part. Interestingly, when the DDI is further increased to $\varepsilon_{\rm dd} = 4$, there are two annular condensates with two annular vortices lines alternately arranged in the dipolar component. The density of scalar component is distributed between the two annular condensates of dipolar component. The condensates of dipolar and scalar components form the ball-and-shell vortex structures. Furthermore, the dipolar component condensate occupies the outside and forms a shell, while the scalar component with small interaction occupies the internal position and forms a ball; these phenomena are shown in the rightmost column of Fig. 2.

3.3. The ground-state vortex structures for $\theta = 0$

Finally, we will consider the case that the polarization is parallel to the condensate plane. For the sake of simplicity, we now assume that the direction of polarization is along the x-axis ($\theta = 0$). In this case, DDI is attractive along the x-direction and repulsive along the y-direction. Figure 3 shows the typical density and phase distributions of this system for varied inter-component interaction, rotation frequency, and DDI. The ground-state vortex structures for slow rotation ($\Omega = 0.7$) are shown in Figs. 3(a) and 3(b), while figures 3(c) and 3(d) are for rapid rotation ($\Omega = 2.5$). The top two rows of Fig. 3 are the density and phase distributions for $\beta = 100$ and $\beta_{12} = 50$, and the bottom two rows are the density and phase distributions for $\beta = 100$ and $\beta_{12} = 250$. The density and phase distributions without DDI can be seen in Figs. 1(a) and 2(a). A weak DDI, such as $\varepsilon_{dd} = 0.5$, can induce a self-induced squeezing of the cloud along the y-axis, because they are attractive in the x-axis direction but repulsive in the y-axis direction; therefore, a vortex line is formed along the x-axis between two semicircle planes. However, the weak DDI in dipolar component and inter-component interaction cannot destroy the rotation symmetry of the scalar component; the density distribution also keeps a ring-like profile, which can be seen from the top two rows of Fig. 3(a). With the increase of DDI to $\varepsilon_{dd} = 3$, one can see from Fig. 3(b) that more and more density stripes and vortex lines are formed and parallel to the x-axis. It is easy to find out that the number of vortices in the dipolar component condensate increases with DDI.

For the rapid rotation ($\Omega = 2.5$) case, the density and phase distributions are shown in the top two rows of Figs. 3(c) and 3(d). More density stripes and vortex lines are formed and paralleled to the x-axis in the dipolar component when the DDI is $\varepsilon_{dd} = 0.5$. The strong centrifugal force produced by rapid rotation repels the dipolar atoms to the outside, while the anisotropic DDI repels them to the y-axis; therefore, most dipolar atoms are repelled outside and form stripes along the x-axis. When the DDI increases to $\varepsilon_{dd} = 3$, the strong DDI can overcome the centrifugal force, and the condensate density in the center increases to the same thickness as that in the edge. Although the density distribution of the dipolar component is obviously changed by the DDI, the density distribution of the scalar component is not changed and kept the profile of ring-like stripe, which is shown in the top two rows of Fig. 3(d).

The bottom two rows of Fig. 3 show the density and phase distributions of the system for the phase separation case with $\beta_{12} = 250$. For slow rotation case ($\Omega = 0.7$) and weak DDI ($\varepsilon_{dd} = 0.5$), the density distributions of dipolar component are squeezed as two stripes along the x-axis, and the dipolar component condensate of the two stripes divides the ring-like condensate of the scalar component into four parts, as shown in the bottom two rows of Fig. 3(a). When the DDI increases to $\varepsilon_{dd} = 3$, four stripes are formed and vortex lines are distributed between them; however, the four parts of scalar condensate are reconnected in the two bottom rows of Fig. 3(b).

For the rapid rotation case ($\Omega = 2.5$), the density and phase distributions are shown in the bottom two rows of Figs. 3(c) and 3(d). It is easy to find out that the weak DDI can induce two high density stripes and three low density stripes, which are alternately arranged. Further increasing the DDI to $\varepsilon_{dd} = 3$, the number of stripes increases and the scope of the stripes becomes smaller and smaller. In addition, three vortex lines are formed among these density stripes. The condensate of scalar component is divided into four parts too.

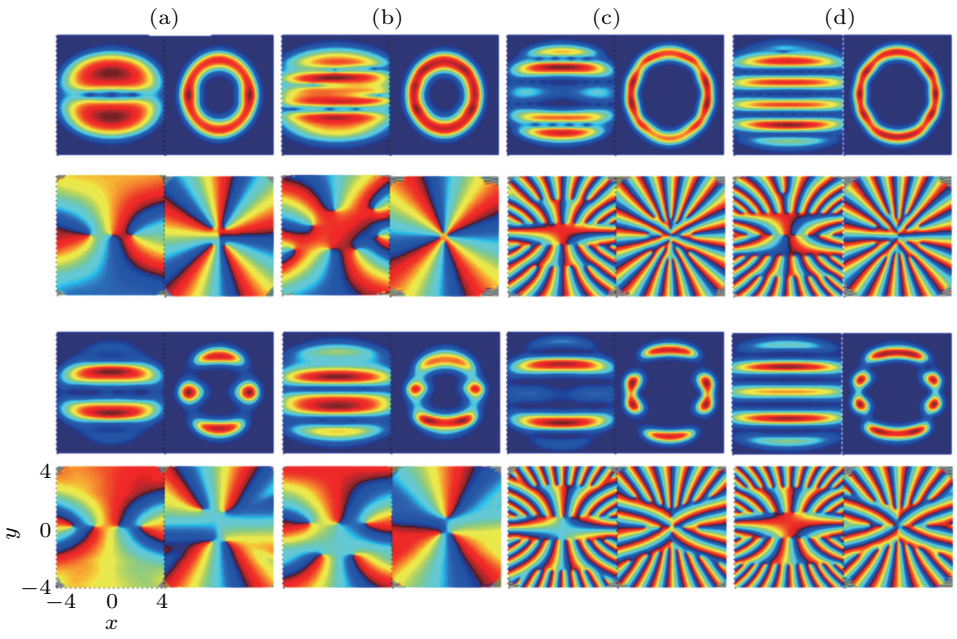


Fig. 3. The typical two-dimensional atomic density and phase profiles of the slow rotation case for different inter-component interactions ($\beta_{12} = 50$ for the top two rows and $\beta_{12} = 250$ for the bottom two rows) and rotation frequencies: (a) and (b) $\Omega = 0.7$, and (c) and (d) $\Omega = 2.5$; for different DDIs: (a) and (c) $\varepsilon_{dd} = 0.5$, and (b) and (d) $\varepsilon_{dd} = 3$. Other parameter is $\theta = 0$.

As discussed in our previous work,[26] ^{52}Cr, ^{164}Dy, and ^{168}Er are candidate for observing the described effects in experiment. Dipolar component 1 and nondipolar component 2 consist of states with spin projections $m_J = -J$ and $m_J = 0$, respectively. The typical particle number is about 10^3–10^5 and the unit length is $a_0 = 1$ μm, which is the typical unit length in BEC experiments. The two-body interaction between atoms can be controlled by modifying atomic collisions through the precise control of scattering lengths by magnetically tuning the Feshbach resonances. The DDI must be combined with the reduction of the contact interaction via the optical Feshbach resonances. Within the existing experimental techniques, these parameters can be realized experimentally.

4. Conclusion

In summary, we have investigated the combined effects of DDI, inter-component contact interaction, and rotation on the ground-state properties of a two-component dipolar BEC confined in a harmonic plus quartic trapping potential. Both slow and fast rotation cases are considered. Different from previous studies, the special external potential considered in the present work allows us to reach fast rotating region. A variety of ground-state vortex structures, including ring-like stripes, square, pentagonal and hexagonal vortex lattice, annular vortices lines, and straight vortex lines, are presented by adjusting the strength and orientation of DDI and the inter-component interaction. Our results show that the DDI is a powerful tool for exploring various topological defects in degenerate quantum gases.

Acknowledgment

Guang-Ping Chen thanks Xiao-Fei Zhang, Wei Han, and Shou-Gang Zhang for helpful discussions.

References

[1] Fetter A L 2009 *Rev. Mod. Phys.* **81** 647
[2] Abo-Shaeer J R, Raman C, Vogels J M and Ketterle W 2001 *Science* **292** 476
[3] Khawaja U A and Stoof H 2001 *Nature* **411** 918
[4] Mühlbauer S, Binz B, Jonietz F, Pfleiderer C and Rosch A 2009 *Science* **323** 915
[5] Mizushima T, Machida K and Kita T 2002 *Phys. Rev. Lett.* **89** 030401
[6] Kasamatsu K, Tsubota M and Ueda M 2004 *Phys. Rev. Lett.* **93** 250406
[7] Bulgakov E N and Sadreev A F 2003 *Phys. Rev. Lett.* **90** 200401
[8] Li Y E and Xue J K 2016 *Chin. Phys. Lett.* **33** 100502
[9] Liu X W and Zhang K Y 2017 *Acta Phys. Sin.* 66 160301 (in Chinese)
[10] Xu T F, Zhang Y F, Xu L C and Li Z D 2017 *Chin. Phys. B* **26** 100304
[11] Zhang H F, Chen F, Yu C C, Sun L H and Xu D H 2017 *Chin. Phys. B* **26** 080304
[12] Griesmaier A, Werner J, Hensler S, Stuhler J and Pfau T 2005 *Phys. Rev. Lett.* **94** 160401
[13] Stuhler J, Koch A T, Fattori M, Pfau T, Giovanazzi S, Pedri P and Santos L 2005 *Phys. Rev. Lett.* **95** 150406
[14] Lahaye T, Koch T, Frohlich B, Fattori M, Metz J, Griesmaier A, Giovanazzi S and Pfau T 2007 *Nature* **448** 672
[15] Lahaye T, Menotti C, Santos L, Lewenstein M L and Pfau T 2009 *Rep. Prog. Phys.* **72** 126401
[16] Kawaguchi Y, Saito H and Ueda M 2006 *Phys. Rev. Lett.* **96** 080405
[17] Zhang X F, Han W, Jiang H F, Saito H and Zhang S G 2016 *Ann. Phys.* **375** 368
[18] Góral K, Rzążewski K and Pfau T 2000 *Phys. Rev. A* **61** 051601
[19] Dong B, Sun Q, Liu W M, Ji A C, Zhang X F and Zhang S G 2017 *Phys. Rev. A* **96** 013619
[20] Góral K, Santos L and Lewenstein M 2002 *Phys. Rev. Lett.* **88** 170406
[21] Vengalattore M, Leslie S R, Guzman J and Stamper-Kurn D M 2008 *Phys. Rev. Lett.* **100** 170403
[22] Chotia A, Neyehuis B, Steven A M, Yan B, Covey J P, Foss-Feig M, Rey A M, Jin D S and Ye J 2012 *Phys. Rev. Lett.* **108** 080405
[23] Wang L X, Dong B, Chen G P, Han W, Zhang S G, Shi Y R and Zhang X F 2016 *Phys. Lett. A* **380** 435
[24] Abad M, Guilleumas M, Mayol R, Pi M and Jezek D M 2010 *Phys. Rev. A* **81** 043619
[25] Zhang X F, Zhang P, Chen G P, Dong B, Tan R B and Zhang S G 2015 *Acta Phys. Sin.* **64** 060302 (in Chinese)
[26] Zhang X F, Han W, Wen L, Zhang P, Dong R F, Chang H and Zhang S G 2015 *Sci. Rep.* **5** 08684
[27] Cozzini M, Jackson B and Stringari S 2006 *Phys. Rev. A* **73** 013603
[28] Hsueh C H, Horng T L, Gou S C and Wu W C 2011 *Phys. Rev. A* **84** 023610
[29] Liu Y and Zhang S Y 2016 *Chin. Phys. B* **25** 090304
[30] Wang H, Wen L H, Yang H, Shi C X and Li J H 2017 *J. Phys. B: At. Mol. Opt. Phys.* **50** 155301
[31] Zhang X F, Wen L, Dai C Q, Dong R F, Jiang H F, Chang H and Zhang S G 2016 *Sci. Rep.* **6** 19380
[32] Zhang Y P, Mao L and Zhang C W 2012 *Phys. Rev. Lett.* **108** 035302
[33] Bao, W Z, Cai Y Y and Wang H Q 2010 *J. Comput. Phys.* **229** 7874